# Experimental study of scaling laws for the complex susceptibility of type-II superconductors

O. F. de Lima and C. A. Cardoso
*Instituto de Física ''Gleb Wataghin,'' UNICAMP, 13083-970 Campinas—SP, Brazil*
(Received 17 May 1999; revised manuscript received 15 November 1999)

Measurements of the nonlinear complex susceptibility $\chi$, taken as a function of amplitude $h$ and frequency $\nu$ of the ac field, can collapse into a single universal curve if they are plotted against the scaling variable $hJ(\nu_{ref})/J(\nu)$, where $J$ is a shielding current density and $\nu_{ref}$ is an arbitrary reference frequency. In this work we present $\chi(h,\nu)$ data for a large range of amplitudes and frequencies, measured in two Nb samples (one single crystal and one polycrystal) and one melt-textured $YBa_2Cu_3O_{7-\delta}$ sample. The predicted scaling relation is verified for several sets of data taken at different temperatures below $T_c$ and applied magnetic fields well above the first critical field $H_{c1}$. Data taken closer to $T_c$ revealed a useful scaling applied directly to the critical current density, evaluated from the peak positions of the imaginary component $\chi''$. The occurrence of different regimes of collective vortex creep is also discussed for the $YBa_2Cu_3O_{7-\delta}$ sample.

## I. INTRODUCTION

The ac susceptibility technique has been widely used to study superconducting materials[1]. Its major advantage is its experimental simplicity, low cost, and great sensitivity. However, quantitative analysis of ac susceptibility data until recently has been somewhat limited and not reliable, due to the lack of theories that consider the actual sample and field geometries occurring in each experiment. Only geometries where demagnetizing effects could be neglected, like infinite cylinders[2] or slabs[3] in parallel applied field, were considered for a long time. Brandt[4,5] has improved considerably this situation by presenting a detailed theory that gives precise results, including flux creep effects, for several finite sample geometries. From the current density **J** he computes the magnetic field **B** inside and outside the sample, the magnetic moment **m**, and the nonlinear and linear ac susceptibilities. An interesting result appears when a periodic excitation field $H(t)=h\sin(\omega t)$ is considered in a strongly nonlinear regime. In this case, if one increases the frequency $\omega$ of the excitation field by a factor of $\phi$ and its amplitude $h$ by a factor of $\phi^{1/\sigma}$, where $\sigma$ is related to the creep exponent, then the complex susceptibility $\chi(h,\omega)$ remains unchanged[6] when normalized to its ideally diamagnetic values for $h\rightarrow 0$ or $\omega\rightarrow\infty$. In this work we present a more general scaling for $\chi(h,\omega)$ that arises when the scaling variable $h/h^*$ is used, where $h^*$ is a characteristic normalization field that depends on sample geometry and on the underlying mechanism for the nonlinear response.[7] In the Bean[8] critical state model (CSM) $h^*=Jd$, $J$ being the screening current density and $d$ a slab half-thickness. It will be shown in Sec. V that in this model Brandt's scaling can be obtained by using a frequency-dependent shielding current, derived within the so-called logarithmic approximation.[9] Our ideas are supported by a large amount of ac susceptibility measurements, for low-critical-temperature ($T_c$) Nb samples (one single crystal and one mechanically deformed polycrystal), as well as for a high-$T_c$ $YBa_2Cu_3O_{7-\delta}$ sample. Therefore, extreme cases of type-II superconductors, displaying from low to high pinning strengths and from weak to strong flux creep effects, were studied in relatively broad temperature ($T$) intervals. Following, in Sec. II we review some basic ideas regarding the scaling law for $\chi(h,\omega)$. In Sec. III the experimental procedure and samples are described. In Sec. IV the experimental results are presented and discussed. Finally, in Sec. V we summarize the main conclusions of this work.

## II. SCALING LAW

Measurements of the complex susceptibility $\chi_m(h,\omega)=\chi'_m+i\chi''_m$ ($m=1,2,\ldots$ labels the various harmonics) require the application of an ac magnetic field $H(t)=h\sin(\omega t)$ to the sample surface. This produces an electric field gradient in the sample interior and induces a shielding current that exerts a Lorentz force on vortices, which are eventually distributed in the sample. Vortices can then be displaced, changing the distribution of magnetic induction $\mathbf{B}(\mathbf{r},t)$ and current density $J(\mathbf{r},t)$. A linear response is characterized when $J$ is proportional to the ac field. In this case the complex susceptibility is independent of $h$ and only its fundamental harmonic is nonzero. Other dependences of $J$ on $h$ lead to nonlinear responses, with an amplitude-dependent susceptibility and nonzero higher harmonics $\chi_m$.

In this paper only the fundamental susceptibility ($m=1$) will be considered; thus we define $\chi(h,\omega)=\chi_1(h,\omega)$. All measured samples will be treated as infinite slabs of thickness $2d$, with the ac and dc magnetic fields applied parallel to their major length. In order to study the scaling laws, measurements were taken mainly in a region of strong nonlinear response, assumed to be caused mainly by bulk pinning. In this case, if $h$ is much smaller than a constant applied field $H_a$, the frequency-dependent current density $J(\omega)$ will be almost constant[10] over a surface shell of thickness $x=(c/4\pi)[h/J(\omega)]$, where $c$ is the velocity of light. Generally speaking this means that when $\chi(h,\omega,T,H_a)$ is measured, keeping $\omega$, $T$, and $H_a$ fixed, then $x$ and $\chi$ become dependent on $h$ only. For $h=h_p$ (full penetration field) the oscillating flux front reaches the center of the sample; hence $x=d$ and $J(\omega)=(c/4\pi)(h_p/d)$. This produces a maximum in the imaginary part $\chi''$, making it very easy to find $h_p$ and to evaluate $J(\omega)$. Notice that the ac penetration length $x$ is the same predicted by the Bean[8] (CSM), but with the static

 

critical current density $J_c$ replaced by $J(\omega)$, which incorporates the effect of flux creep.

For a partial penetration of the applied ac field ($x \leqslant d$ or $h \leqslant h_p$), the fundamental harmonic of the complex susceptibility reads[1,8]

$$\chi(h,\omega)=\left(-1+\frac{ch}{8\pi J(\omega)d}\right)+i\left(\frac{ch}{6\pi^2 J(\omega)d}\right). \qquad (1)$$

Therefore, provided that measurements are taken in a sufficiently nonlinear region where the CSM applies, one should expect a coincidence of the $\chi(h,\omega)$ curves when plotted as a function of the scaling variable $h/Jd$.

### III. SAMPLES AND EXPERIMENTAL DETAILS

The samples employed in this work were two high-purity (>99.9%) Nb bars, both having the same dimensions $1\times1\times3$ mm$^3$, and a melt-textured-grown $YBa_2Cu_3O_{7-\delta}$ (YBCO-MTG) cut into a parallelepiped shape having dimensions $1.1\times2.5\times2.7$ mm$^3$.

The YBCO-MTG sample was characterized in previous works[11–13] and has $T_c=91.8$ K. It contains a dense array of platelike grains with a typical cross section of $400\times80$ $\mu$m$^2$ in the *a-b* plane of the orthorhombic structure. All grains are well-aligned along the *c* axis direction within an angular spread around 2°. The measurements presented here were made with the ac and dc magnetic fields applied in the direction parallel to the sample *c* axis.

One of the Nb bars is a single crystal[14] having $T_c=9.25$ K and was cut from a long cylinder with 3.4 mm diameter oriented along the [110] direction. The other Nb bar has $T_c=9.39$ K and was cut from a mechanically deformed rod of polycrystalline material. Both bars were etched and chemically polished in order to remove a shell about 500 $\mu$m thick of damaged material, which has a much higher $\kappa$ (Ginzburg-Landau factor) when compared to the bulk value.[15]

All measurements were performed in a commercial PPMS (Physical Properties Measurement System) made by the Quantum Design Co. Several sets of $\chi$ measurements were taken as a function of $h$ (0.1–17 Oe) for fixed frequencies $\nu$ ranging from 50 Hz to 10 kHz. The data were normalized such that $4\pi\chi'(h,\omega)=-1$ when $h\to0.1$, corresponding to the horizontal region for lower values of $h$ in the $\chi\times h$ curves. Before taking each $\chi\times h$ curve a magnetic field $H_a \gg H_{c1}(T^*)$ was applied to the sample in the normal state ($H_{c1}$ is the lower critical field). Following this, the sample was then cooled down to the measuring temperature $T^*$. This procedure aimed at establishing a fully penetrated flux distribution in the entire sample.

### IV. RESULTS AND DISCUSSION

In this paper we present results for $H_a=500$ Oe only. However, for the YBCO-MTG sample a field $H_a=5000$ Oe was also tested, providing additional confirmation for the amplitude-frequency scaling law. In all figures the dashed lines connecting experimental points are only guides to the eyes. Fits to the data will be identified properly when needed.

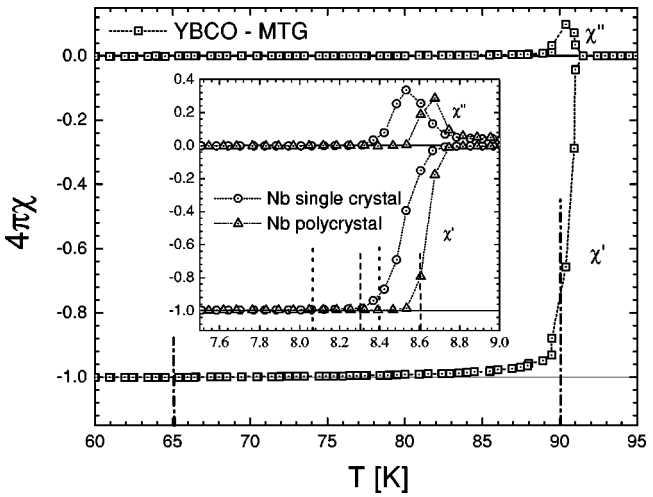


FIG. 1. Complex susceptibility as a function of temperature for the YBCO-MTG sample and Nb samples (inset). The experimental parameters were $H_a=500$ Oe, $h=5$ Oe, and $\nu=1000$ Hz, respectively, the constant applied field, amplitude of the excitation field, and frequency. Vertical lines indicate the temperature window used for each sample: Nb single crystal (dotted line), Nb polycrystal (dashed line), and YBCO-MTG (dot-dashed line).

Figure 1 shows $4\pi\chi\times T$ for all three samples. It helps to identify the temperature window employed in each case: from 8.05 K to 8.40 K for the Nb single crystal, from 8.30 K to 8.60 K for the Nb polycrystal, and from 65 K to 90 K for the YBCO-MTG. Within these temperature intervals $\chi(h,\omega)$ is sufficiently nonlinear, as required in the present study. However, by approaching the lower-temperature limit a crossover to the linear regime is observed, especially for small amplitudes of the ac field. The limit at higher temperatures is very close to the maximum of $\chi''$ where a melted or depinned state of the vortices is expected to occur,[10,16] making pinning interactions irrelevant and leading to a linear response again.

Figure 2 provides experimental evidence for the strong nonlinear response of $\chi$, measured with $\nu=5000$ Hz ($\omega=2\pi\nu$), between 85 K and 90 K, for sample YBCO-MTG. This figure demonstrates that the CSM applies quite well to this data, following a test introduced by Civale *et al.*[17] Every horizontal line (fixed value of $\chi'$) corresponds to a constant value of the ac penetration length *x*, according to Eq. (1). On the other hand, $J(\omega)$ in this experiment is a function of $T$ only, so every vertical line corresponds to a constant value of $J(\omega,T,H_a)$. Hence, $J(P)=J(Q)$, where $P$ and $Q$ are points located at the crossing between the vertical line at $T\approx89$ K and the $\chi'$ curves for $h=4$ Oe ($P$) and $h=2$ Oe ($Q$). The neighbor point $R$ belongs to the $\chi'$ curve for $h=8$ Oe and has the same ac penetration $x$ as for point $P$. Since the CSM establishes that $J_c\propto h/x$, we get $J_c(R)=2J_c(P)$ because $h(R)=2h(P)$. Similarly, $J_c(S)=2J_c(Q)$, where $S$ and $Q$ belong, respectively, to the $\chi'$ curves for $h=4$ Oe and 2 Oe (see Fig. 2). From the preceding equalities we get $J_c(R)=J_c(S)$, implying that points $R$ and $S$ should be at the same $T$ (same vertical line), as is indeed verified experimentally. Therefore, the occurrence of several rectangles similar to PQSR represents a graphical

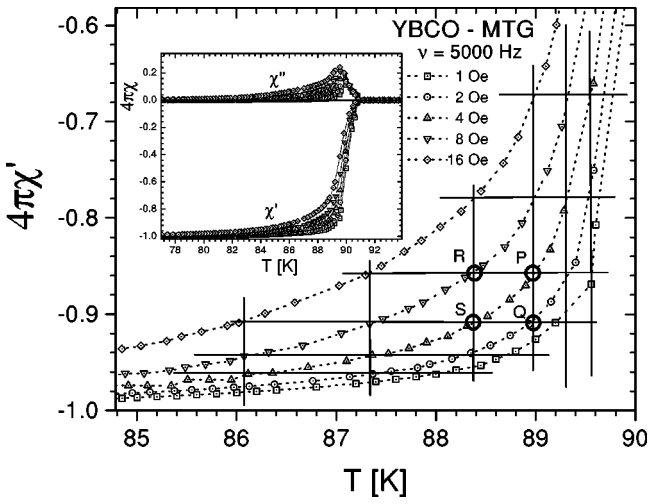


FIG. 2. Graphical test for the validity of the Bean critical state model in a strongly nonlinear regime of the complex susceptibility, for the YBCO-MTG sample (see text). The inset gives a full view of the real and imaginary parts of $\chi$.

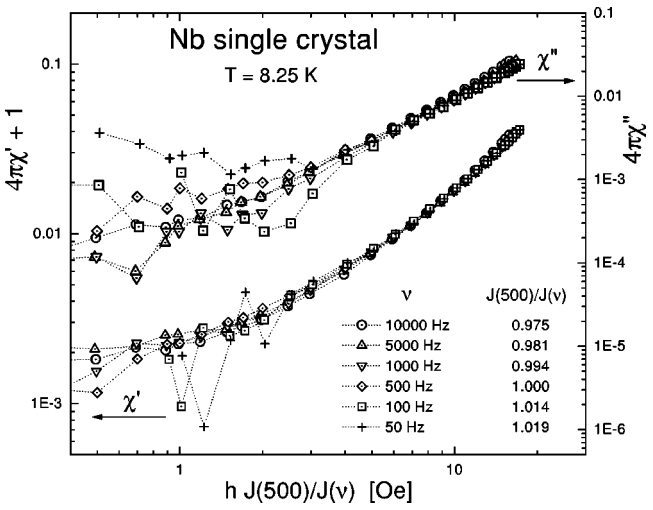


FIG. 3. Complex susceptibility as a function of the scaled amplitude, for the Nb single crystal at $T=8.25$ K. The scaling factor $J(500)/J(\nu)$ is the ratio between the shielding current density for the reference frequency $\nu_0=500$ Hz and a chosen $\nu$. This result is typical for most of the central part of the temperature window defined in Fig. 1.

proof of applicability of the CSM. Notice that this proof is not precisely verified for the lowest value $h=1$ Oe, possibly because this amplitude is approaching the crossover to a linear response. We have also validated the graphical proof for the Nb polycrystal and single crystal (not shown here), thus making sure that the CSM applies to the nonlinear regime of all samples studied here. Actually it is a well-accepted fact that even for high-$T_c$ superconductors the straight line approximation for the flux profiles works very well under alternating fields.[3,10,17,18] For instance, Qin and Yao[18] have demonstrated this fact by numerically solving the flux creep equation for the frequency range between 0.1 Hz and 100 kHz and found that $J(\omega)=(c/4\pi)(h_p/d)$ is a good approximation in the fully penetrated state.

To test the amplitude-frequency scaling law we have plotted the $\chi(h,\nu)$ data against a more convenient scaling variable $\tilde{h}=hJ(500)/J(\nu)$, instead of using $\tilde{h}=h/(Jd)$ as proposed initially. Here, $J(500)$ is a normalizing shielding current for the arbitrary reference frequency $\nu_{ref}=500$ Hz. The practical fitting operation consists of finding the appropriate multiplicative factor $J(500)/J(\nu)$ that transforms the horizontal scale $h$ of each measured curve $\chi'(h,\nu)$, in order to superimpose it with the reference curve $\chi'(h,500$ Hz). In all cases the imaginary component $\chi''(h,\nu)$ is expected to collapse automatically into a single universal curve by using the same fitted factor $J(500)/J(\nu)$. By this procedure the frequency-dependent current density $J(\nu)$ can be determined after a careful evaluation of $J(500)$, as will be done later in this paper.

Figures 3, 4, and 5 show double-logarithmic plots of $4\pi\chi(h,\nu)$ as a function of $\tilde{h}$ for the three measured samples. In order to span the vertical scale (left axis) close to $4\pi\chi'=-1$ we have used the more appropriate variable $4\pi\chi'+1$. We see what appears to be a crossover from linear to nonlinear response at $\tilde{h}\approx 3$ Oe for the Nb samples (Figs. 3 and 4) and $\tilde{h}\approx 0.9$ Oe for the YBCO-MTG sample (Fig. 5). This observation applies for the frequency interval between 100 Hz and $10^4$ Hz. For $\tilde{h}$ above the crossover region all $\chi(h,\nu)$ data collapse very well into a single universal curve, validating the scaling law. This scaling clearly is not verified for $\tilde{h}$ below the crossover region, where the response becomes linear. In this low $\tilde{h}$ region the as-measured $\chi$ curves overlap very well for each sample as should be expected in a linear regime. It is worth noticing that below $\tilde{h}\approx 1$ Oe dispersion of the data points increases due to a deterioration of the signal-to-noise ratio. This happens particularly for $\nu<500$ Hz, since the voltage signal induced on the measuring pickup coils gets close to the equipment sensitivity. It is interesting to notice also that in the nonlinear regime all curves shown in Figs. 3 –5 approach nicely to straight lines with slopes around 1. Actually this is expected from a double

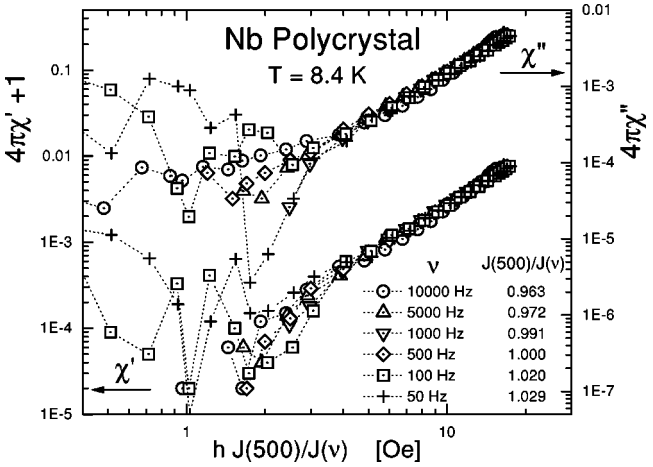


FIG. 4. Complex susceptibility as a function of the scaled amplitude (see caption of Fig. 3), for the Nb polycrystal at $T=8.4$ K. This result is typical for most of the central part of the temperature window defined in Fig. 1.

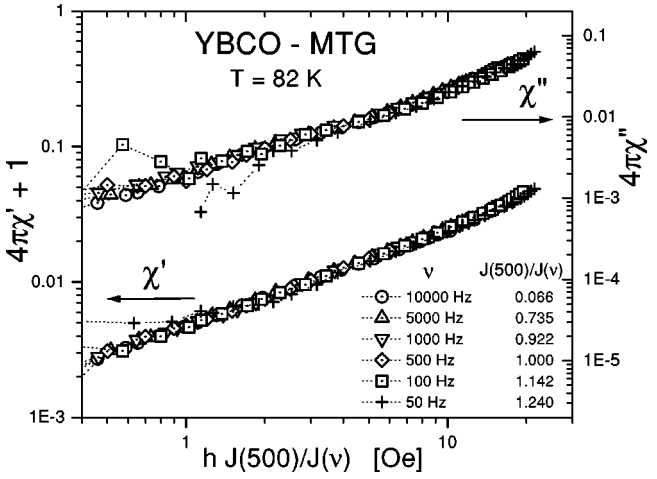


FIG. 5. Complex susceptibility as a function of the scaled amplitude (see caption of Fig. 3), for the YBCO-MTG sample at $T = 82$ K. This result is typical for most of the central part of the temperature window defined in Fig. 1.

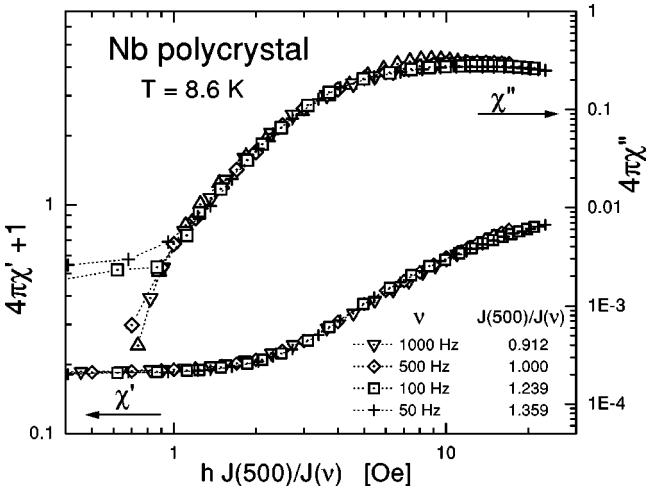


FIG. 7. Complex susceptibility as a function of the scaled amplitude (see caption of Fig. 3), for the Nb polycrystal at $T = 8.6$ K. This result is typical for the upper part of the temperature window defined in Fig. 1.

logarithmic plot of Eq. (1), which substantiates the validity of the Bean CSM.

The measurements displayed in Figs. 3–5 are typical for $T$ in the central region of the temperature window as specified in Fig. 1. For higher $T$ (see Figs. 6–8), getting close to the depining-melting line,[16] the amplitude-frequency scaling is verified also, although the $\chi''(h,\nu)$ curves do not collapse very well around the peak region. Data scattering is particularly visible for sample YBCO-MTG (see Fig. 8). A similar anomalous increase in the peak heights of $\chi''$, proportional to $h$, was also reported without explanation by Fàbrega *et al.*[19] We suspect that when $\nu$ or $h$ is increased in this region of very intense flux creep[20] (especially for the YBCO-MTG sample) self-heating effects caused by power loss[21] $P \propto h^2\nu^{1/2}$ become relevant. A slight increase of the sample temperature, in the region below and near the peak of $\chi''$, thus promotes an increase of $\chi$ even for fixed $\nu$ and $h$ values. Indeed, we have confirmed this fact by observing a $T$ increase of about 0.5 K measured with a thermometer located near the sample, while the system thermometer, placed $\sim 5$ cm below the sample, was reading stable. Our equipment is similar to most temperature variable systems, where the sample exchanges heat through a low pressure ($\sim 10$ mtorr) helium gas atmosphere, so temperature control gets worse if sample self-heating occurs.

A remarkable feature appearing in Figs. 6–8 is the precise coincidence of the $\chi''$ peak positions, although the different $\chi'' \times h$ curves, in some cases, are far from collapsing into a single universal curve. It is worth stressing that the observed coincidence of $\chi''$ peak positions arises automatically when the fitting procedure is applied to the real component $\chi'$. In our view this result provides good evidence for the amplitude-frequency scaling law applied directly to the critical current density. This can be of great help in the charac-

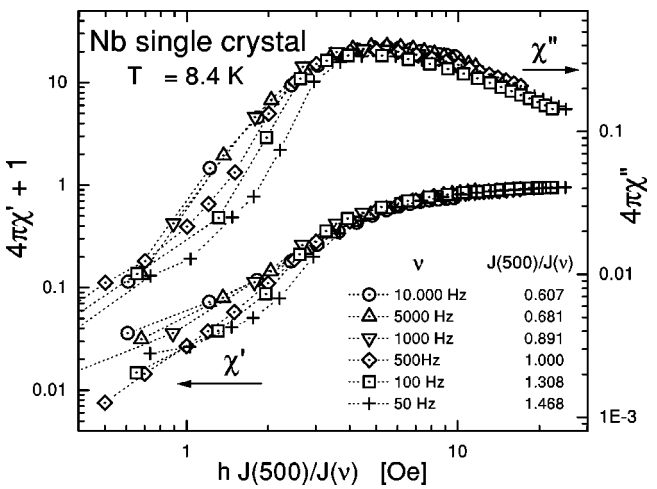


FIG. 6. Complex susceptibility as a function of the scaled amplitude (see caption of Fig. 3), for the Nb single crystal at $T = 8.4$ K. This result is typical for the upper part of the temperature window defined in Fig. 1.

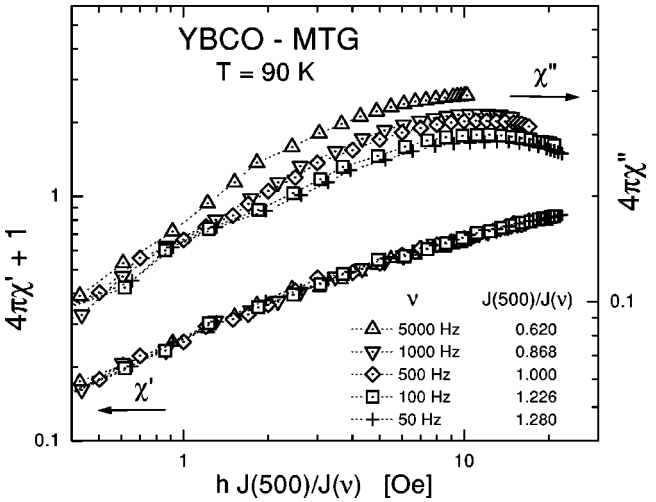


FIG. 8. Complex susceptibility as a function of the scaled amplitude (see caption of Fig. 3), for the YBCO-MTG sample at $T = 90$ K. This result is typical for the upper part of the temperature window defined in Fig. 1.

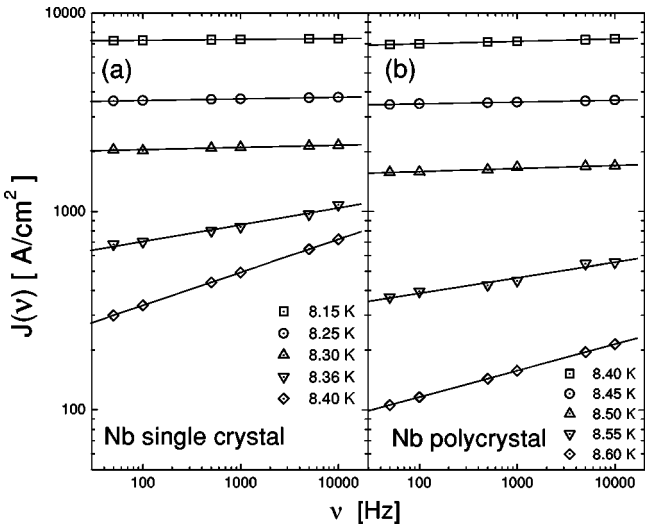


FIG. 9. Double-logarithmic plot of the current density $J$ as a function of frequency $\nu$ of the ac field, for $H_a = 500$ Oe. The solid lines represent linear fits consistent with the logarithmic approximation for the activation energy $U = U_c \ln(J_c/J)$ (see text).

terization of materials for practical applications, when ac currents and fields are involved.

### Current density $J(\nu)$ and creep exponent $n(T,H)$

If the absolute value of $J(500)$ is evaluated, we then get immediately $J(\nu)$ for all measured $T$, using the fitted values $J(500)/J(\nu)$ which are listed in the legends of Figs. 3–8. These figures show experimental data for only two representative temperatures for all samples. However, several other temperatures were employed in this work to test the scaling law. The reference values $J(500)$ were evaluated for all measured $T$ using $J(500) = (c/4\pi)(h_p/d)$ [or $J(500) = 5h_p/(2\pi d)$ in practical units of A/cm$^2$], where $h_p$ is the amplitude of the ac field at the peak of $\chi''$ for $\nu = 500$ Hz. Figures 9(a) and 9(b) show $J(\nu,T) \times \nu$, respectively, for the Nb single crystal and Nb polycrystal. The solid lines represent excellent linear fits to the experimental points; hence $\ln J(\nu,T) \propto \ln(\nu)$. This latter relation confirms the formula[22,23]

$$J(\nu,T,H) = J_c(T,H)\left(\frac{\nu}{\nu_0}\right)^{1/n}, \qquad (2)$$

where $n(T,H) = U_c(T,H)/kT$ is the creep exponent, $U_c(T,H)$ is an activation energy, $k$ is the Boltzmann constant, and $\nu_0$ is a normalizing frequency, interpreted by Fàbrega *et al.* as an intrinsic attempt frequency of vortex jumps.[19,22] Equation (2) was derived from a general expression $J(\nu,T,H) = J_c(T,H)g\{kT\ln(\nu_0/\nu)/U\}$ which incorporates a frequency dependence on the static $J_c$ given by the CSM.[8] The function $0 < g\{y\} < 1$ describes the effective reduction of the critical current density during one period of the ac field, and depends on the regime of thermally activated flux motion. In the so-called logarithmic approximation[9] $U = U_c(T,H)\ln(J_c/J)$, and[22] $g\{y\} = \exp(-y)$, thus leading to Eq. (2).

According to Eq. (2) the slopes of the fitted straight lines in Fig. 9 (for the Nb samples) and inset of Fig. 10 (for the YBCO-MTG sample) give $1/n$. The creep exponent $n$ decreases, going from lower to higher temperatures, as shown in Fig. 11 for all the three samples. Actually this indicates the relevance of flux creep,[4] such that for a smaller value of $n$ corresponds a higher creep rate.

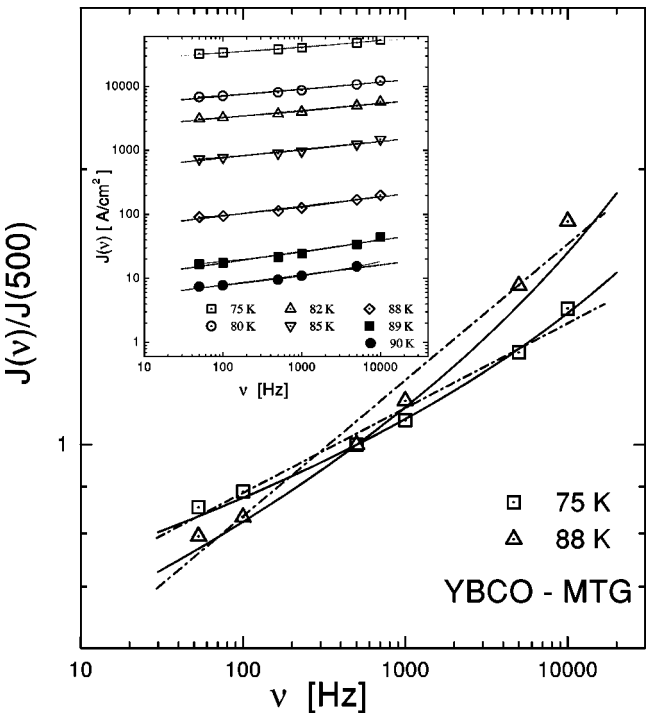


FIG. 10. Double-logarithmic plot of the normalized current density $J(\nu)/J(500)$ as a function of frequency $\nu$. This figure shows better fits using Eq. (4) (solid lines) than using Eq. (2) (straight dot-dashed lines). The inset shows $J(\nu) \times \nu$ for all measured temperatures.

A close inspection of Fig. 10 reveals a gradual deviation of the linear fits (dash-dotted lines) for the YBCO-MTG data, as $T$ increases. The double-logarithmic plot of $J(\nu,T) \times \nu$ is shown in the inset, while the main plot shows $J(\nu)/J(500) \times \nu$ (for $T = 75$ and 89 K) in order to magnify the mentioned deviation. Much better fits, represented by solid lines in Fig. 10, were obtained using the following expression derived from the collective flux creep[16,24] and vortex-glass[25] theories:

$$J(\nu,T,H) = J_c(T,H)\left[\frac{kT}{U_c(T,H)}\ln\left(\frac{\nu_0}{\nu}\right)\right]^{-1/\mu}, \qquad (3)$$

where $\mu$ is a small positive factor that depends on the flux creep regime.[16] Here, $g\{y\} = y^{-1/\mu}$ and $U = U_c(J/Jc)^{-\mu}$; therefore $J(\nu,T,H) = J_c(T,H)g\{y\}$ leads to Eq. (3).

In terms of the normalized current density, for $T$ and $H$ constants, one gets

$$\frac{J(\nu)}{J(500)} = \left[\frac{\ln(\nu_0/\nu)}{\ln(\nu_0/500)}\right]^{-1/\mu}. \qquad (4)$$

The best fits of this equation to the data were obtained using free parameter values $\nu_0 \sim 4 \times 10^5$ Hz and $0.8 < \mu < 1.3$, as shown in the inset of Fig. 11(b). The values found for $\nu_0$ corroborate the interpretation of this characteristic frequency

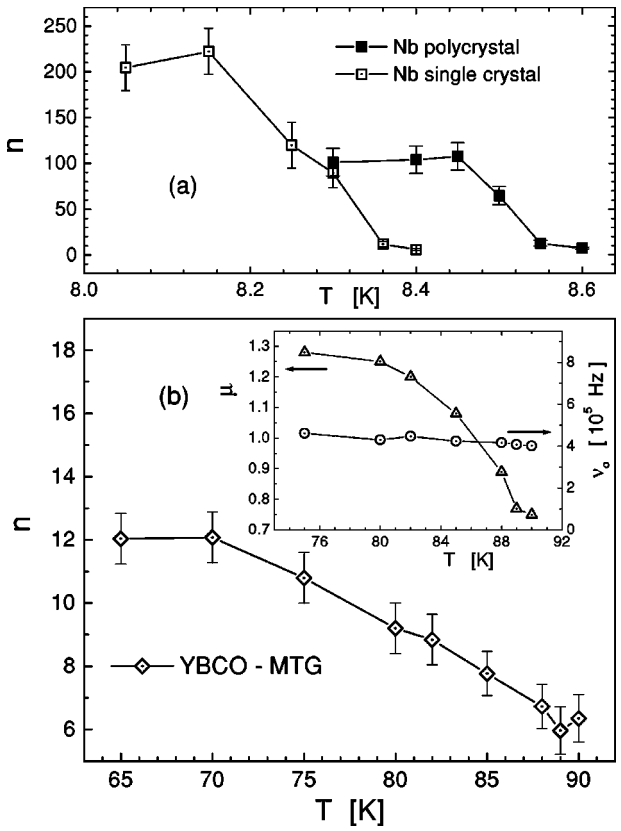


FIG. 11. The creep exponent $n$, for all samples, decreases with temperature consistently with an expected increase of vortex creep rate. The inset of (b) displays the temperature dependence of the fitting parameters $\mu$ (left axis) and $\nu_0$ (right axis) from Eq. (4) (see text).

as a macroscopic and extrinsic quantity[24,26] instead of a microscopic and intrinsic quantity, which would imply[22] $\nu_0 \sim 10^9$ Hz. On the other hand, a monotonic decrease of $\mu$ with $T$, similar to that shown in the inset of Fig. 11(b), has also been reported by Sun *et al.*[27] in a study using YBCO-MTG samples. Following the collective creep model,[16] we could say that while $T$ increases between $\sim 75$ K and 90 K the vortex system changes from a small bundle regime ($\mu = 5/2$), passing through an intermediate bundle regime ($\mu = 1$), reaching the large bundle regime ($\mu = 7/9$) at the highest $T \gtrsim 89$ K (for $H_a = 500$ Oe). The occurrence of these different regimes is expected to be consistently shifted to lower $T$ values, for higher dc fields $H_a$.[16,27]

The evolution from creep of small to large vortex bundles corresponds to progressively smaller shielding currents in the sample. Actually this can be observed through vertical cuts of the curves in Figs. 9 and 10, which give $J(T)$ for fixed $\nu$ and $H_a$ values. This type of analysis based on the collective flux creep model is very interesting. However, it is important to be aware of the narrow time window $t_w = 1/\nu$ ($\sim 10^{-2}$–$10^{-4}$ s) probed in our ac susceptibility measurements. This might not be compatible with usual studies that rely on long time relaxation of the magnetization. Therefore, more work is still needed in this area of vortex dynamics.

## V. CONCLUDING REMARKS

Although the creep exponent $n(T,H)$ has proved to be a very useful concept,[4,28,29] one should be cautious about its application. The best way of defining $n$ is through a current-voltage power law $E \propto J^n$, used to describe the nonlinear relationship between electric field $E$ and current density $J$. However, this power law fits well to experimental data only if an effective creep exponent is considered such that sample inhomogeneity[28,30] and frequency effects are neglected or averaged. For instance, we have found[6] that Brandt's scaling[4,5] $\tilde{h} = h(\nu_{ref}/\nu)^{1/\sigma}$ works well only for the low-$T_c$ Nb samples, where the frequency effect on $n$ is negligible. In fact the preceding equation is readily found, with $\sigma = n$, if one combines Eq. (2) with the scaling variable $\tilde{h} = hJ(\nu_{ref})/J(\nu)$ introduced in this paper. Then, the excellent linear fits shown in Fig. 9 can be viewed as an equivalent verification of Brandt's scaling for the Nb samples. For the YBCO-MTG sample (Fig. 10) frequency effects are clearly stronger, requiring a more general scaling law like the one introduced here.

We have assumed in this paper that bulk pinning was the main cause for the nonlinear response observed in all samples. This assumption is supported by the graphical test depicted in Fig. 2, as well as by the almost symmetrical shape of the hysteretic $M$ vs $H$ curves (not shown here). However, for the YBCO-MTG sample it is also possible that surface barrier effects could be the cause for the observed nonlinear response.[31,32] In this case the vortex dynamic properties discussed here for YBCO would not apply, although the scaling of $\chi$ would be preserved.

Concluding, in this work we presented experimental evidence for a scaling law relating amplitude and frequency in the complex susceptibility, to both low- and high-$T_c$ superconductors. One single crystalline and one polycrystalline samples of Nb, as well as one melt-textured-grown YBCO sample were measured under a constant field $H_a = 500$ Oe, for amplitudes of the ac field between 0.1 and 17 Oe and frequencies between 50 Hz and 10 kHz. Measurements were taken at several temperatures, within appropriate temperature windows, such that a strongly nonlinear response was assured. For all samples the ac susceptibility data collapsed very well into a single universal curve when plotted against the scaling variable $\tilde{h} = hJ(\nu_{ref})/J(\nu)$, which is based on the Bean critical state model. In particular, we have shown a direct scaling of the critical current density $J_c$, related to the coincidence of the dissipative peaks in the imaginary component $\chi''$. We expect that $J_c$ values determined by transport-current measurements might also present the same behavior, a result that could be of interest for the area of applications.

## ACKNOWLEDGMENTS

We acknowledge Y. Kopelevich, V. P. S. Awana, and Chris Lobb for stimulating discussions. This work was supported by Brazilian agencies Fundação de Amparo a Pesquisa do Estado de São Paulo (FAPESP) through Contract Nos. 95/4721-4 and 97/00794-2, and Conselho Nacional de Pesquisas (CNPq) through Contract No. 300465/88-2.

[1] See, e.g., *Magnetic Susceptibility of Superconductors and Other Spin Systems*, edited by R. A. Hein, T. L. Francavilla, and D. H. Liebenberg (Plenum, New York, 1991).
[2] J. R. Clem, H. R. Kerchner, and S. T. Sekula, Phys. Rev. B **14**, 1893 (1976).
[3] L. Ji, H. R. Sohn, G. C. Spalding, C. J. Lobb, and M. Tinkham, Phys. Rev. B **40**, 10 936 (1989).
[4] E. H. Brandt, Phys. Rev. B **58**, 6506 (1998).
[5] E. H. Brandt, Phys. Rev. B **58**, 6523 (1998).
[6] C. A. Cardoso and O. F. de Lima, in *1999 Centennial Meeting of the American Physical Society* [Bull. Am. Phys. Soc. **44**, 1283 (1999)].
[7] For instance, $h^* = J\delta/\pi$, for a thin strip or film of thickness $\delta$ in a perpendicular field. In this case superconducting irreversible effects are mainly determined by geometrical barrier effects (see Ref. 31).
[8] C. P. Bean, Phys. Rev. Lett. **8**, 250 (1962); Rev. Mod. Phys. **36**, 31 (1964).
[9] E. Zeldov, N. M. Amer, G. Koren, A. Gupta, M. W. McElfresh, and R. J. Gambino, Appl. Phys. Lett. **56**, 680 (1990).
[10] C. J. van der Beek, V. B. Geshkenbein, and V. M. Vinokur, Phys. Rev. B **48**, 3393 (1993).
[11] R. de Andrade, Jr. and Oscar F. de Lima, Phys. Rev. B **51**, 9383 (1995).
[12] O. F. de Lima and R. de Andrade, Jr., Physica C **248**, 353 (1995).
[13] F. M. Araújo-Moreira, W. A. Ortiz, and O. F. de Lima, Physica C **311**, 98 (1999).
[14] A. S. Brito, G. Zerweck, and O. F. de Lima, J. Low Temp. Phys. **36**, 33 (1979).
[15] O. F. de Lima, M. A. Avila, and C. A. Cardoso, Physica C **282-287**, 2201 (1997).
[16] G. Blatter, M. V. Feigel'man, V. B. Geshkenbein, A. I. Larkin, and V. M. Vinokur, Rev. Mod. Phys. **66**, 1125 (1994).
[17] L. Civale, T. K. Worthington, L. Krusin-Elbaum, and F. Holtzberg, in *Magnetic Susceptibility of Superconductors and Other Spin Systems* (Ref. 1), p. 313.
[18] M. J. Qin and X. X. Yao, Phys. Rev. B **54**, 7536 (1996).
[19] L. Fàbrega, J. Fontcuberta, S. Piñol, C. J. van der Beek, and P. H. Kes, Phys. Rev. B **47**, 15 250 (1993).
[20] Y. Yeshurun and A. P. Malozemoff, Phys. Rev. Lett. **60**, 2202 (1988).
[21] J. R. Clem, in *Magnetic Susceptibilities of Superconductors and Other Spin Systems* (Ref. 1), p. 177.
[22] L. Fàbrega, J. Fontcuberta, L. Civale, and S. Piñol, Phys. Rev. B **50**, 1199 (1994).
[23] B. J. Jönsson, K. V. Rao, S. H. Yun, and U. O. Karlsson, Phys. Rev. B **58**, 5862 (1998).
[24] M. V. Feigel'man, V. B. Geshkenbein, A. I. Larkin, and V. M. Vinokur, Phys. Rev. Lett. **63**, 2303 (1989).
[25] M. P. A. Fisher, Phys. Rev. Lett. **62**, 1415 (1989).
[26] Y. Abulafia, A. Shaulov, Y. Wolfus, R. Prozorov, L. Burlachkov, Y. Yeshurun, D. Majer, E. Zeldov, and V. M. Vinokur, Phys. Rev. Lett. **75**, 2404 (1995).
[27] Y. R. Sun, J. R. Thompson, Y. J. Chen, D. K. Christen, and A. Goyal, Phys. Rev. B **47**, 14 481 (1993).
[28] J. Z. Sun, C. B. Eom, B. Lairson, J. C. Bravman, and T. H. Geballe, Phys. Rev. B **43**, 3002 (1991).
[29] J. W. Ekin, Cryogenics **27**, 603 (1987).
[30] A. Gurevich and V. M. Vinokur, Phys. Rev. Lett. **83**, 3037 (1999).
[31] Shi Li, M. Fistul, J. Deak, P. Metcalf, G. F. Giuliani, and M. McElfresh, Phys. Rev. B **52**, 739 (1995).
[32] C. J. van der Beek, M. V. Indenbom, G. D 'Anna, and W. Benoit, Physica C **258**, 105 (1996).